# Photocatalytic Degradation Of Fast Green Dye Under Visible Light By Strontium Doped Nickel β−Hydroxide (Sr/Ni(OH)$_2$) Nanoparticle

**Dr. Satishkumar Damodar Thakare[1], Niraj Satish Thorat[2]**

Department of Chemistry
Karm. Ramraoji Aher Arts, Science & Commerce College
Deola Dist. Nashik.

**Abstract:**
**Strontium doped Nickel hydroxide (Sr/Ni(OH$_2$) nanoparticles, pure NiO were synthesized by co-precipitation method with the use of $NiCl_2.6H_2O$, $Sr(NO_3)_2$ for Nickel and Strontium sources, respectively. NaOH used as a precipitating agent. The impact of Sr doping agent on both morphological and characteristics of nanoparticles was investigated using XRD, SEM, and FTIR methods. The co-precipitation approach was the most efficient and cost-effective way to synthesize nanoparticles. Sr/Ni(OH)$_2$ was synthesized at a low temperature and is employed in photo-degradation applications. The photo-catalytic degradation of dyes has been investigated all throughout the world, independent of national scientific standards. Common factors to mention for degradation investigations are dye content, oxidizing species concentration, catalyst employed, strength, and photon source. The synthesized NiO, Sr/Ni(OH)$_2$ served as an effective catalyst for the photo-degradation of Fast green (FG) dye. Photo-catalytic degradation of rapid green dye used first-order kinetics, and dye degradation produced the greatest results. The photo-degradation efficiency of the rapid green dye was around 50.64% for NiO and 95.2% for the produced Sr/Ni(OH)$_2$ catalyst. The kinetic data collected during the decolorization of the fast-green dye were examined.**

**Keywords: Strontium-doped Nickel hydroxide, Nanoparticles, Nickel oxide (NiO), Photo-catalysis, Photo-degradation, Dye degradation, Fast Green (FG) dye, Morphological characterization, Environmental remediation.**

## INTRODUCTION

There are two primary techniques for nanoparticle synthesis: top-down and bottom-up.
The Top-Down approach entails reducing bigger materials to nanoparticles by destructive procedures such as mechanical grinding, melt mixing, and laser ablation. Mechanical milling uses high-temperature steel balls to compress metal powders into nanoparticles, whereas melt mixing produces nanocrystals inside metallic glasses. Laser ablation uses laser beams in a liquid media to produce stable nanoparticles.

The Bottom-Up approach generates nanoparticles from atomic or molecular precursors using techniques such as Physical Vapor Deposition (PVD), Sol-Gel, and Chemical Vapor Deposition (CVD). PVD regulates nanoparticle size by gas interactions in a vacuum chamber, Sol-Gel synthesis allows for low-temperature nanoparticle creation, and CVD distributes thin coatings onto a substrate through chemical reactions at regulated temperatures.

Nanoparticles have several uses, including medicine delivery, genetic detection, and antibacterial therapies. Their unique qualities help to progress medicine, tissue engineering, and biotechnology. Nickel oxide (NiO) nanoparticles, which have a cubic lattice structure, are widely employed in catalysis, battery cathodes, gas sensors, and magnetic materials, with a particular emphasis on dye-sensitized photocathodes. Their defect structure makes them a strong p-type semiconductor, ideal for gas detection and phenol degradation. Nickel hydroxide (Ni(OH)$_2$) nanoparticles are white, spherical metal particles with a large surface area (130-

150 $m^2/g$). They are available in high purity and carbon-coated forms. They have two phases: α-$Ni(OH)_2$ (cubic structure) and β-$Ni(OH)_2$ (hexagonal structure)[4].

A photo-catalyst is a material that induces a photo-catalytic reaction upon exposure to light without undergoing any permanent change. Photo-catalysis refers to a photo-induced reaction facilitated by a catalyst but does not directly accelerate the reaction rate [6].
It is classified into two types:

- Homogeneous catalysis – The photo-catalyst and reactant exist in the same phase (e.g., dyes, coordination compounds, and natural pigments).
- Heterogeneous catalysis – The photo-catalyst and reactant exist in different phases, with examples including transition metal chalcogenides, which exhibit unique properties [6]

Photo-dye degradation is essential for removing toxic organic dyes from industrial wastewater, as dyes are highly visible, carcinogenic, and harmful to aquatic life. Conventional methods like adsorption and coagulation only transfer dyes into solid waste, causing secondary pollution [7-9]. Photo-catalysis has emerged as an effective and eco-friendly alternative for water purification, using semiconducting photo-catalysts to break down organic molecules through oxidation-reduction reactions. Photo-catalysts exist in various forms, such as nanoparticles, nanowires, 2D and 3D structures, and their efficiency is enhanced due to high surface area [12-16]
Fast green is also called as food green. The molecular formula of fast green is $C_{37}H_{34}N_2O_{10}S_3Na_2$, and its molar mass is 808.85 g/mol. The structure of fast green dye is given below in figure 1.7. In histology and cytology, fast green dye is commonly used. It has been shown to cause tumours in laboratory animals and to cause mutations in both experimental animals and humans. It also has the potential to irritate the pupils, scalp, digestive tract, and respiratory tract in its undiluted form [17].

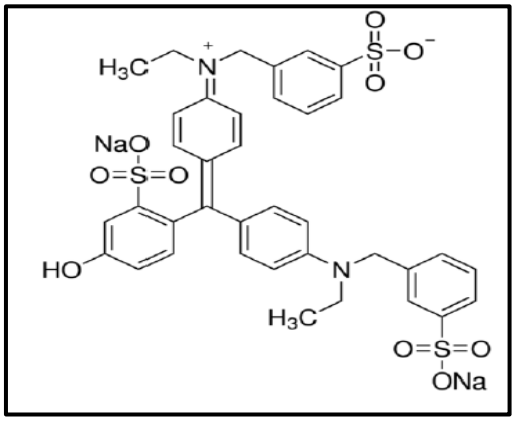


**Fig.1. Structure of Fast Green dye**

**MATERIALS AND METHODS:**
Pure nickel oxide and strontium doped nickel hydroxide nanoparticles were prepared using the co-precipitation process, and their material characteristics were examined.

**MATERIALS**:
All compounds used in this experiment were analytical grade and did not require additional purification. Merck supplied the nickel (II) chloride hexahydrate ($NiCl_2.6H_2O$), SRL supplied the sodium hydroxide pellets (NaOH), SRL supplied the strontium nitrate ($Sr(NO_3)_2$), SRL supplied the polyvinylpyrrolidone (PVP), and SRL supplied the ethanol and acetone. All of these solutions were made with deionized water.

**EXPERIMENTAL METHODS**
**Synthesis of NiO:**
Nickel oxide nanoparticles were synthesized via the co-precipitation approach, which involves the thermal breakdown of nickel hydroxide ($Ni(OH)_2$). In a 250ml beaker, place approximately 0.5M of Nickel (II)

chloride hexahydrate and add 50ml of deionized water. To that mixture, 1g of PVP is added, with the goal of reducing particle size and preventing agglomeration.
The reaction mixture is agitated in a magnetic stirrer for nearly 2 hours at room temperature. The product is then completely rinsed with deionized water to eliminate any remaining residues, followed by an acetone wash. Finally, the sample is dried at 160°C in an air oven before being calcined to 450°C in a muffle furnace. When calcinated, the colour of the sample changes from green to black. The resultant thus obtained is the Nickel oxide nanoparticle.

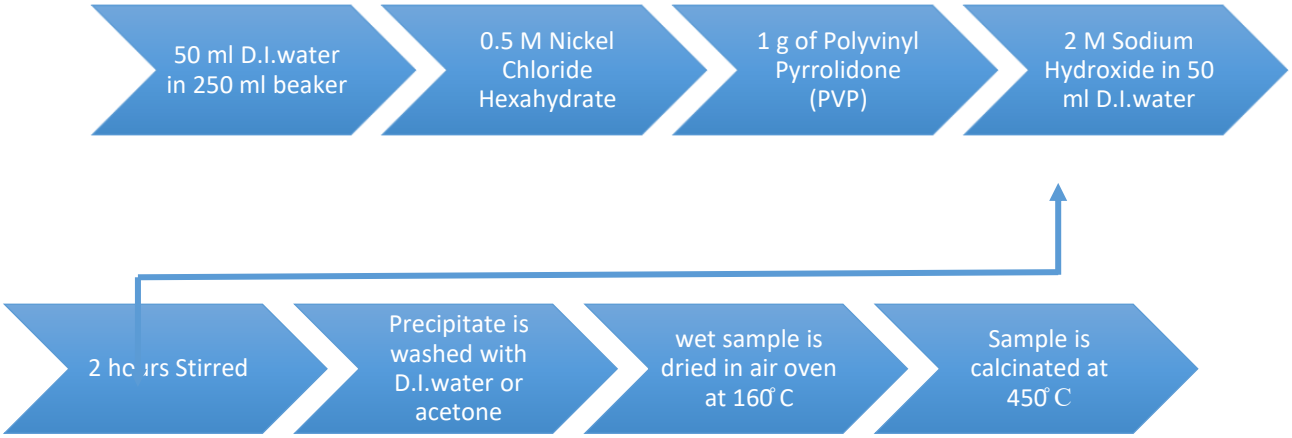


**Fig.2. Flow diagram of synthesis of NiO**

**SYNTHESIS OF STRONTIUM DOPED NICKEL HYDROXIDE NANOPARTICLE (Sr/Ni(OH)$_2$ ):**
250ml beaker is taken with 50ml of deionized water and to that 0.5M of Nickel (II) chloride hexahydrate and 1g of polyvinyl pyrrolidone are added. To that mixture, 5% of strontium nitrate is added and stirred for 30 minutes in a magnetic stirrer. The temperature was maintained for about 80°C. Then 2M of sodium hydroxide pellets were weighed using a digital balance and was dissolved in 50ml deionized water and it is added drop by drop slowly into the mixture.
As the solution is continuously stirred, the colour of the solution changes from dark green colour to light green. Stirring is continued for almost 2 hours. Then a green coloured precipitate appears at the bottom of the beaker. The precipitate is then washed thoroughly with deionized water and acetone a number of times. Then the precipitate was dried at 160°C in hot air oven. The finally obtained sample is the Strontium doped Nickel hydroxide nanoparticle (Sr/(Ni(OH)$_2$) [16].

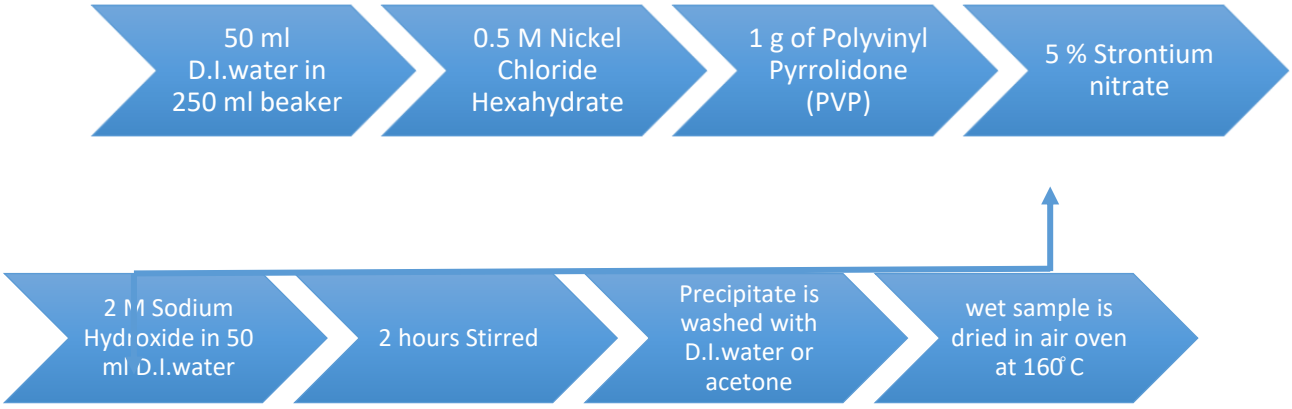


**Fig.3. Synthesis of Sr/Ni(OH)$_2$**

**CHARACTERIZATION TECHNIQUES:**
The crystal structure, morphology, compositional information, organic functional groups on the surface, and photo-catalytic application of the produced nanoparticles were investigated utilizing the following equipment.

These include X-ray diffraction (XRD), scanning electron microscopy (SEM), and Fourier Transform Infrared spectroscopy (FTIR). This project work presents the approaches that have been emphasized. The next part contains a brief discussion of the techniques mentioned above [18].
X-ray Diffraction (XRD) is a widely used non-destructive technique for analyzing the structural properties of nanoparticles. It provides information on phase, crystallinity, chemical composition, unit cell symmetry, lattice constants, stress, strain, and growth orientation. Since 90% of solid materials are crystalline, XRD serves as a fingerprint for material identification [1-2].

The technique works by irradiating a material with monochromatic X-rays of a wavelength similar to the interatomic distance, causing diffraction based on Bragg's equation ($n\lambda = 2d \sin \theta$) [42]. The intensity and pattern of scattered light depend on the atomic arrangement, making XRD a valuable tool for studying the structure and properties of nanoparticles.
Scanning Electron Microscopy (SEM) is a high-resolution technique used to characterize the size and shape of nanoparticles. It provides 2D images with detailed structural information that can be modeled to recreate 3D structures with high precision. SEM imaging is based on secondary electrons (SEs) and backscattered electrons (BSEs) generated when a sample is bombarded by a primary electron (PE) beam at an accelerating voltage of around 30 kV. SEs have a low escape depth (~a few nm) due to their low energy, while BSEs have a slightly higher escape depth. With the growing application of nanoparticles in commercial products, the demand for SEM in laboratories for nanoparticle characterization is increasing [20-21].

Fourier Transform Infrared (FTIR) Spectroscopy is a non-destructive technique used for surface characterization of nanoparticles. It helps determine the chemical structure and surface reactive sites under specific conditions. FTIR reveals the bonds and structural composition of nanoparticles and can analyze various sample types, including liquids, solids, pastes, powders, and fibers. It is useful for both quantitative and qualitative analysis of materials [22-23].

However, overlapping IR absorption bands pose a challenge in FTIR characterization, making it difficult to identify certain functional groups, despite the availability of computer-searchable databases for analysis.

**RESULTS AND DISCUSSION:**
The crystal structure, morphology, compositional information, organic functional groups on the surface, and photo-catalytic application of the produced nanoparticles were investigated utilizing the following equipment. These include X-ray diffraction (XRD), scanning electron microscopy (SEM), and Fourier Transform Infrared spectroscopy (FTIR). This project work presents the approaches that have been emphasized. Figure 5 (a) depicts a photocopy of NiO in black, whereas figure (b) depicts a green sample containing $Ni(OH)_2$. The following section provides a quick overview of the strategies mentioned above.

**Figure 4(a) NiO Sample**


**4(b) Sr/$Ni(OH)_2$ sample**

**1) X-Ray Diffraction (XRD):**
When a material is irradiated with monochromatic light of wavelength about the material's interatomic distance, the light is scattered by the atoms and interferes, resulting in diffracted light of increased intensity.

The arrangement of atoms in the material influences the intensity of dispersed light. Bragg's equation states that if the incidence angle is θ and the wavelength of light is λ, constructive interference occurs at an angle of 2θ from the incident beam Bragg's equation is given by,

$$n\lambda = 2d \sin\theta$$

Where, n is the diffraction order, d is the distance between the diffracting planes and θ is the Bragg's angle. Generally, in XRD Cu- K□ is the incident light for which the λ = 1.5405 nm. Distance between the diffracting planes is calculated according to Bragg's equation and indexed by comparing it with the d spacing of the material from the Joint Committee on Powder Diffraction Standards (JCPDS) data.

NiO spheres exhibits several well-defined diffraction reflections at 19.01°, 31.72°, 38.63°, 45.458°, 51.97°, 59.21° and 75.18°. The XRD of bare Ni substrate, which shows peaks at 45°, 55° and 75°. The diffraction peaks for NiO are shown in planes of (111), (200), (220), (311) and (222) are shown in Figure 4.1. All these diffraction peaks can be perfectly indexed to the cubic (FCC) crystalline structure of NiO, and also their relative intensity of the characteristic peaks, which is in accordance with the standard spectrum (JCPDS, No. 04-0835).

The XRD pattern reveals that the samples are single phase, with no other diffraction peaks other than the characteristic peaks of the cubic lattice of NiO. This result indicates that the physical phases of NiO nanoparticles are pure, and were prepared and discussed in detail [24].

Strontium doped nickel hydroxide shows peaks at (001), (100), (101), (110), (111), (200) planes.

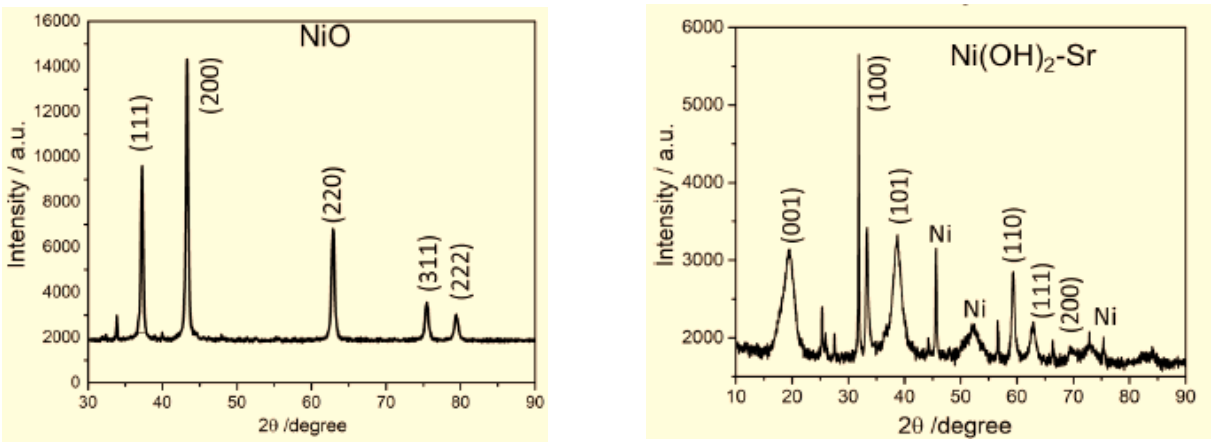


**Figure 5. XRD peak for NiO and Sr/Ni(OH)$_2$**

The crystallite size of the Strontium doped nickel hydroxide nanoparticle is found out using Debye-Scherrer's formula,

$$D = k\lambda/\beta \cos\theta$$

Where k is the empirical constant which is equal to 0.9, λ is the wavelength of X-ray radiation (1.5405 Å for Cu-Kα), β is the full width at half maximum of the diffraction peak and θ is the peak position [6].

The crystallite sizes of Sr/Ni(OH)$_2$ samples is found to be 8.7 nm which was calculated from the measured values from the data.

**2) Scanning Electron Microscope (SEM):**

A high-resolution scanning electron microscope (SEM) is ideal for determining the size and form of nanoparticles since sample preparation and image analysis are rapid and straightforward. [25] SEM pictures allowed for a comprehensive investigation of the nanoparticles' morphological structure [26]. The scanning electron microscope works similarly to an optical microscope, except rather than collecting photons, it detects electrons dispersed from the material. Electrons can have shorter wavelengths than photons because they can be accelerated by an electric field. As a result, the SEM can magnify images up to 200,000 times [27]The morphological changes in the synthesised sample nanoparticles were identified and analyzed. Nickel oxide analysed by SEM is shown in figure 6(a). Sr doped nickel hydroxide nanoparticles thus synthesised at low temperature was analysed and the images are displayed in Figure 6(b).

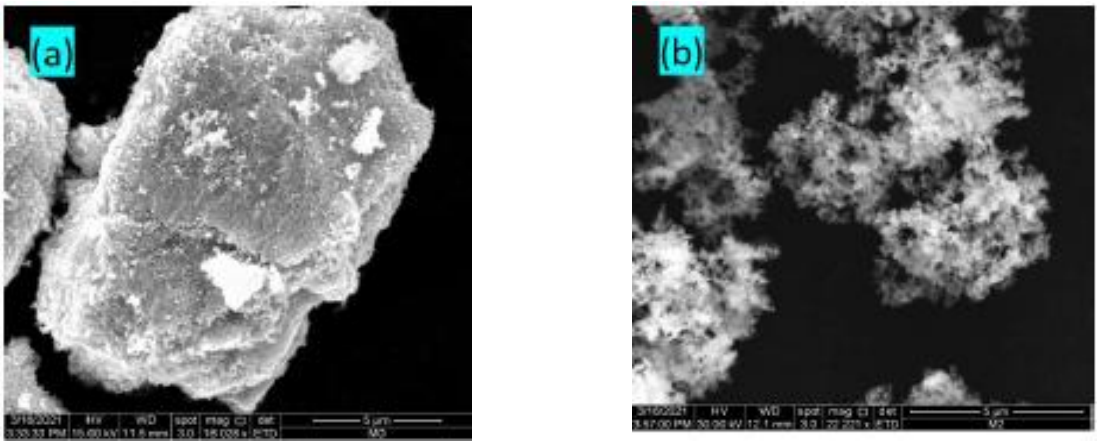


**Figure 6(a) Scanning electron microscopy (SEM) image of pure NiO nanoparticles and 6(b) SEM image of Sr doped $Ni(OH)_2$ nanoparticles. The SEM images were measured for both the powder samples (NiO and Sr doped $Ni(OH)_2$. The powder samples were pasted on the carbon tape for measuring the SEM images**

Nickel oxide has a higher surface energy than strontium doped nickel hydroxide because it is agglomerated [28]. Compared to pure nickel oxide, strontium doped nickel hydroxide has limited structures. The results demonstrate that the synthesized NiO nanoparticles are smooth, spherical in form, and some are agglomerated due to their high surface area to volume ratio and lower cohesive energy than the bulk materials. SEM images of strontium-doped nickel hydroxide are spherical. Strontium doped nickel hydroxide is smaller in size than pure nickel oxide due to its strong dispersion Nickel oxide can be de-agglomerated by calcining at a higher temperature of around 160°C According to SEM pictures, strontium doped nickel hydroxide may have a size of less than 10nm

**3) Fourier Transform Infra-Red Spectroscopy:**

The FTIR analysis of nickel oxide and strontium doped nickel hydroxide is shown in the figure 7 below. The formation of the nanoparticles can be observed from its colour change. The vibrational peak at 3488 cm-1 is due to the O-H stretch and the peak around 578 cm-1 is described as the Ni-O stretching vibration.

The broad absorption band in the region 500-600 cm-1 is the Ni-O stretching vibration. The size of the samples used in this study is less than the bulk forms of NiO. The broad spectrum at 3450 cm-1 is due to the O-H stretching vibrations and a weak band at 1645 cm-1 is the H-O-H bending vibrations [31].

The broad band at 3440 cm-1 is the stretching vibration of water molecules present in the nickel hydroxide nanoparticle. The figure 7(b) shows the peaks of FT-IR of strontium doped nickel hydroxide.

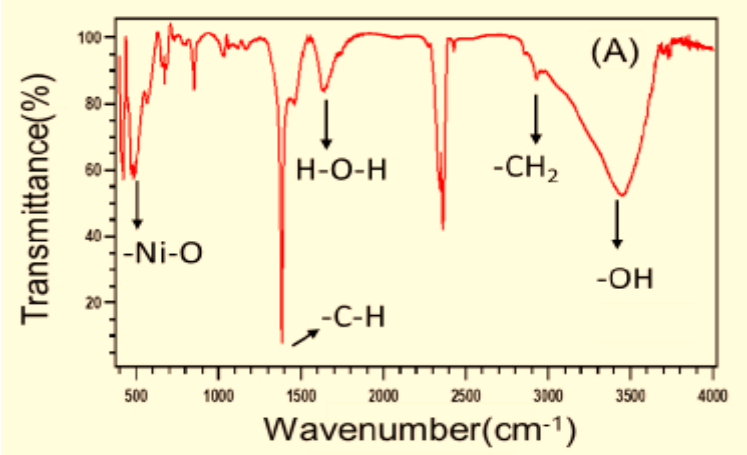

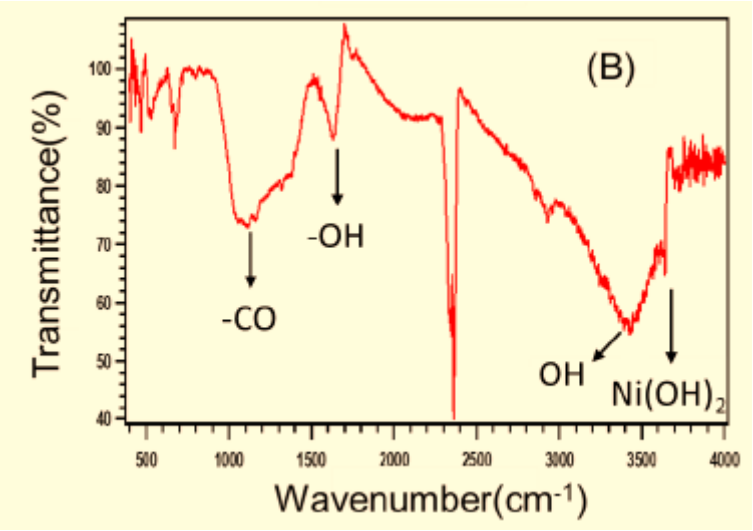


**Figure 7 (a) FT-IR peak of NiO and 7(b) FT-IR peak of Sr/Ni(OH)$_2$**

**4) Photo-catalytic Activity Test:**

Fast green (FG) was chosen as the model organic pollutants to test the photo-catalytic dye degradation analysis for the catalyst. Typically, a catalyst (20 mg) was added into the 50 ml of aqueous dye solution (20 mg L-1) then, the dye solution was kept in dark room to attain the adsorption and desorption equilibrium of dyes on surface of catalyst. Then, the dye solution was irradiated on sunlight for overall time period of 120 minutes. 2 ml of solution was taken at appropriate interval of time. The collected solution was centrifuged and filtered using a 0.2 µm syringe filter. The degradation efficiency is determined by the degradation of organic dyes on UV-Vis spectrophotometer. The degradation efficiency is calculated by the formula,

Degradation efficiency (%) = $C\text{-}C_0/C$ x100 …… (1)

where C and $C_0$ are the initial and final concentrations of dye molecules.

After 1st completed the photo-catalytic reaction, the catalyst was collected by centrifuge and washed with water and dried at 70oC. The regenerated catalyst was used to evaluate the stability and reusability of the catalyst by degradation the dye solution.

The first order kinetic reaction value were used to determine the correct degradation rate of FG as follows;

$$-\ln(C/C_0) = kt \quad \ldots\ldots\ldots\ldots\ldots\ldots (2)$$

where, k = rate of reaction constant and t is time

The Photo-catalytic dye degradation activity were performed during the well sun shining between 11:00 AM to 2:00 PM in clear sky. The average solar light intensity was measured about 1.00 x 105 lux. Likewise, the effect of some other important operational parameters such as pH of dye solution and catalyst dosage study were performed. In the pH test, dye solution pH was adjusted by the addition of 0.1 M hydrochloric acid solution and 0.1M of sodium hydroxide solution.

**6) Photo-catalytic Activity:**

The photo-catalytic degradation efficiency of as prepared catalysts of NiO, and Sr/Ni(OH)2 nanoparticles were resolute by the deprivation of FG dye under irradiation of Sun light. When irradiating the FG dye solution, the concentration of the dye was noticeably reduced and it was confirmed by the significant color variation.

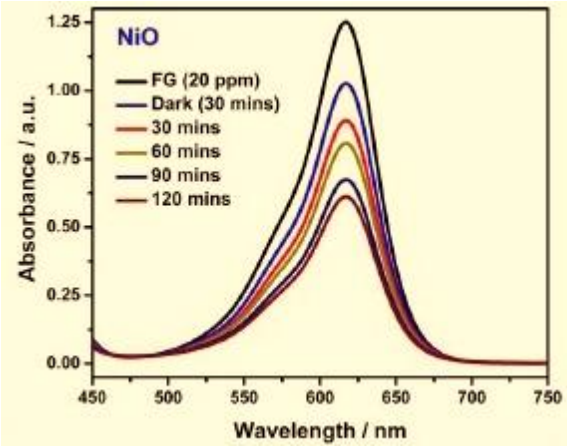


Figure 8(a)

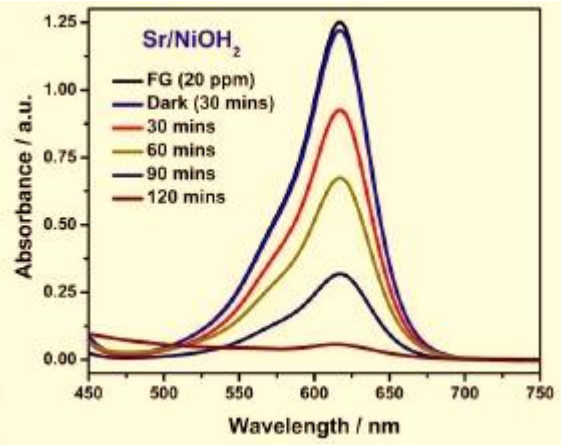


Figure 8(b)

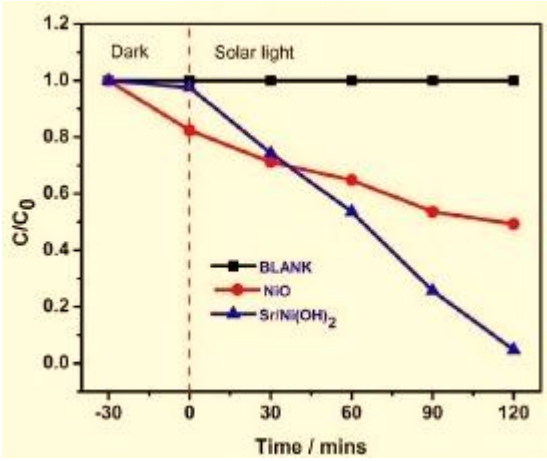


Figure 8(c)

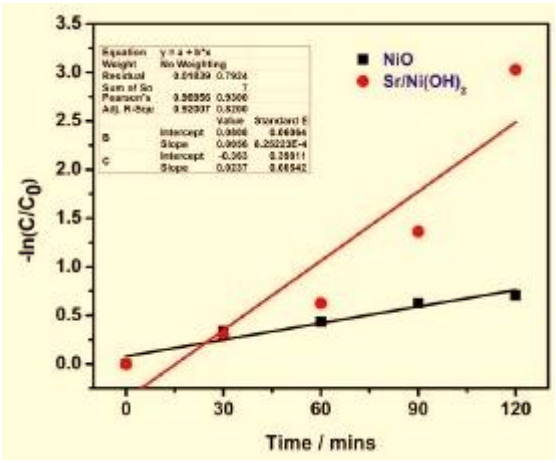


Figure 8(d)

**Figure 8 (a-b) represents the UV-visible spectra for the FG with occurrence of catalysts NiO, and Sr/ Ni(OH)$_2$ were irradiated by sun light for 120 minutes. 8(c) C/C0 versus time interval plot of FG dye 8(d) –ln (C/C0) versus time interval plot of FG dye**

For NiO catalyst, the catalyst influences the organic molecule to achieve the efficiency of about 50.64% within 120 mins. The photo-catalyst experiment was further extended to doped samples. The degradation reaction of Sr/ Ni(OH)$_2$ samples were performed by the same process. The rate of electron-hole pair recombination was delayed by doping the metal ions into the NiO structure results increased the degradation efficiency. Compared to NiO catalyst, Sr/Ni(OH)$_2$ catalysts reached high efficiency of degradation of 95.2%, respectively [32].

The significant improvement of the degradation efficiency is due to the doping effect of Sr ion at the Ni2+ lattice sites, it reduce recombination of excited charge carriers (electron-hole pair). Figure 8(c) depicts the changes in initial and final concentration of dye in the presence and absence of photo-catalyst against the light irradiation with respect to time (t) for the FG dye solution. The Sr/Ni(OH)$_2$ catalyst shows highest degradation ability due to the fact that sub energy-level act as traps for recombination. Based on the sub energy level of the conduction band helps to produce a large number of reactive oxygen species (ROS). In addition the investigation of pseudo-first order kinetics studies shown in Figure 8(d) the degradation rates were 0.0112 min-1 and 0.0375 min-1 for NiO, and Sr/ Ni(OH)$_2$ nanoparticles against FG dye, respectively. From the studies rate constant value and R2 values are listed in Table.1. The Figure 8 shows schematic diagram illustrating the mechanism of charge separation, generation of reactive oxygen species (ROS) and photocatalytic activity of photocatalyst under sunlight irradiation [33].

The mechanism of FG dye degradation for the $Sr/Ni(OH)_2$ catalyst is described as follows,

(i) Formation of electron hole pair

$Sr/Ni(OH)_2 + h\nu \longrightarrow h^+ (VB) + e^- (CB)$ (3)

(ii) Formation of hydroxyl radicals

$OH^- + h^+ \longrightarrow OH^-$ (4)

$H_2O + h^+ \longrightarrow OH^- + H^+$ (5)

(iii) Formation of superoxide radicals

$O_2 + e^- \longrightarrow O_2^-$ (6)

(iv) Photo-degradation of crystal violet and rhodamine B dye

$Dye + OH^- + O_2 \longrightarrow$ Degradation Products (7)

**Table 1** Photo-catalytic activity result of NiO, and Sr/ $Ni(OH)_2$ nanoparticles

| Sr.No. | Catalyst | Band Gap (eV) | **Degradation efficiency (%) (120 minutes)** | **K ($min^{-1}$)** | **$R^2$** |
|---|---|---|---|---|---|
| **Fast green (20 ppm)** | | | | | |
| 1 | NiO | 3.21 | 50.64 | 0.012 | 0.920 |
| 2 | Sr/Ni(OH)2 | 2.82 | 95.2 | 0.054 | 0.820 |

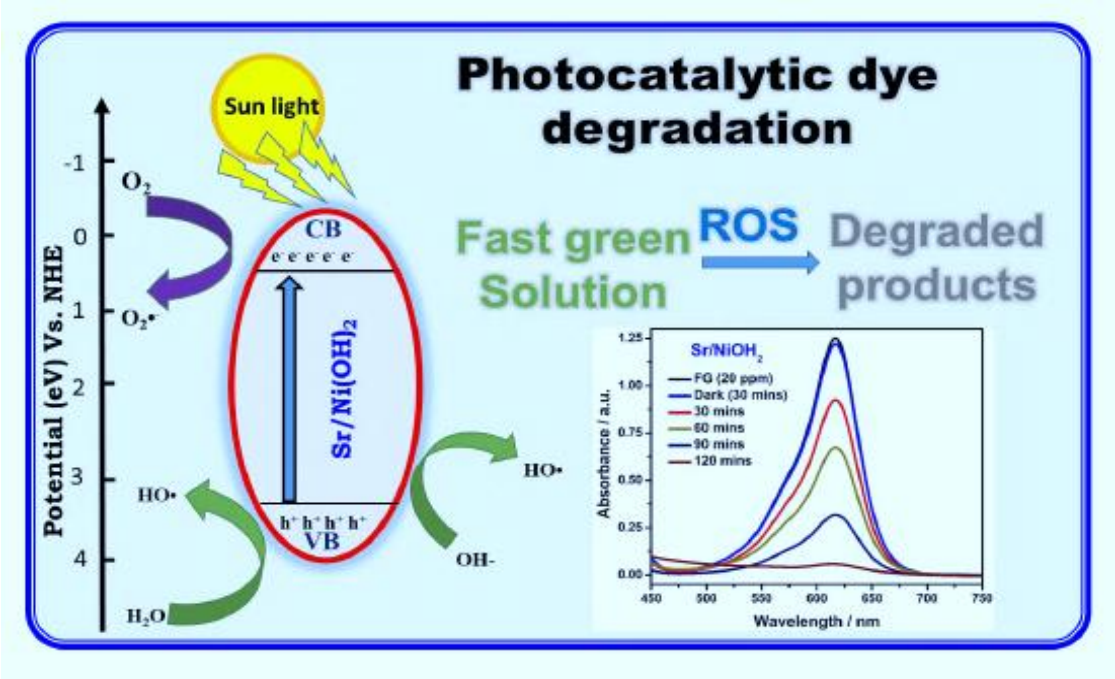


**Figure 9. Schematic diagram illustrating the mechanism of charge separation and photo-catalytic activity of photo-catalyst under the sunlight irradiation**

## SUMMARY AND CONCLUSION:

Nickel-based metal oxides have been gaining popularity due to their applications in catalysis, dye degradation, battery cathodes, antiferromagnetic layers, p-type transparent conducting films, and electro-chromic films. Polyvinylpyrrolidone has been used as a surfactant to decrease particle size. Here, a high temperature-based cubic phase of NiO nanoparticles was produced. $Ni(OH)_2$ was initially synthesized using the chemical precipitation technique, and the wet sample was subsequently calcined at 450°C for 4 hours in an air environment.

Chemical precipitation was used to create Sr (5%) ion-doped $Ni(OH)_2$ nanoparticles with a low temperature hexagonal configuration. The structure and dimensions were validated using XRD. The crystallite size was computed using the Debye Scherrer formula; the size was determined to be 14.3 nm and 8.7 nm for NiO and Sr doped $Ni(OH)_2$ nanoparticles, respectively. The SEM microscopy revealed that the produced nanoparticles were in the nanoscale range and had a spherical form. The organic functional groups on the surface of the nanoparticles were identified using FT-IR spectroscopy. The photo-catalytic results indicated that Sr doped $Ni(OH)_2$ had better dye degradation of Fast green (FG) than pure NiO nanoparticles due to efficient charge carrier generation followed by free radical synthesis during light irradiation. Thus, the generated cost-effective and low-temperature Sr doped Nickel hydroxide nanoparticle $Sr/Ni(OH)_2$ may be a promising option for water purification by photo-catalysis.

**REFERENCES:**


1) Ealia, S. Anu Mary, and M. P. Saravanakumar. "A review on the classification, characterisation, synthesis of nanoparticles and their application." In *IOP Conference Series: Materials Science and Engineering*, vol. 263, no. 3, p. 032019. IOP Publishing, 2017.
2) Cartaxo, Ana Luísa Pécurto. "Nanoparticles types and properties–understanding these promising devices in the biomedical area." (2010).
3) Fernández-García, Marcos, and José A. Rodriguez. "Metal oxide nanoparticles." *Encyclopedia of inorganic and bioinorganic chemistry* (2011).
4) El-Kemary, M., N. Nagy, and I. El-Mehasseb. "Nickel oxide nanoparticles: synthesis and spectral studies of interactions with glucose." *Materials Science in Semiconductor Processing* 16, no. 6 (2013): 1747-1752.
5) Ohtani, Bunsho, and Tsukasa Torimoto. "Photocatalysts.", 2016.
6) Ameta, Rakshit, and Suresh C. Ameta. *Photocatalysis: principles and applications*. 2016.
7) Chiu, Yi-Hsuan, Tso-Fu Mark Chang, Chun-Yi Chen, Masato Sone, and Yung-Jung Hsu. "Mechanistic insights into photodegradation of organic dyes using heterostructure photocatalysts." *Catalysts* 9, no. 5 (2019): 430.
8) Chen, S.; Zhang, J.; Zhang, C.; Yue, Q.; Li, Y.; Li, C. Equilibrium and kinetic studies of methyl orange and methyl violet adsorption on activated carbon derived from Phragmites australis. Desalination 2010, 252, 149–156.
9) Daneshvar, N.; Salari, D.; Khataee, A.R. Photocatalytic degradation of azo dye acid red 14 in water: Investigation of the effect of operational parameters. J. Photochem. Photobiol. A Chem. 2003, 157, 111–116.
10) Ledakowicz, S.; Gonera, M. Optimisation of oxidants dose for combined chemical and biological treatment of textile wastewater. Water Res. 1999, 33, 2511–2516. [23]. Grzechulska, J.; Morawski, A.W. Photocatalytic decomposition of azo-dye acid black 1 in water over modified titanium dioxide. Appl. Catal. B Environ. 2002, 36, 45–51.
11) Aleboyeh, A.; Aleboyeh, H.; Moussa, Y. “Critical” effect of hydrogen peroxide in photochemical oxidative decolorization of dyes: Acid Orange 8, Acid Blue 74 and Methyl Orange. Dyes Pigments 2003, 57, 67–75.
12) Ayodhya, D.; Veerabhadram, G. A review on recent advances in photodegradation of dyes using doped and heterojunction based semiconductor metal sulfide nanostructures for environmental protection. Mater. Today Energy 2018, 9, 83–113.
13) Chaturvedi, Shalini, and Pragnesh N. Dave. "Environmental application of photocatalysis." In *Materials Science Forum*, vol. 734, pp. 273-294. Trans Tech Publications Ltd, 2013.
14) Bhati, Indu, Pinki B. Punjabi, and Suresh C. Ameta. "Photocatalytic degradation of fast green using nanosized CeCrO 3." *Macedonian Journal of Chemistry and Chemical Engineering* 29, no. 2 (2010): 195-202.
15) Anwer, Hassan, Asad Mahmood, Jechan Lee, Ki-Hyun Kim, Jae-Woo Park, and Alex CK Yip. "Photocatalysts for degradation of dyes in industrial effluents: Opportunities and challenges." *Nano Research* 12, no. 5 (2019): 955-972.
16) Yang, Xiaogang, and Dunwei Wang. "Photocatalysis: from fundamental principles to materials and applications." *ACS Applied Energy Materials* 1, no. 12 (2018): 6657-6693. [33] Bhati, Indu, Pinki B.

Punjabi, and Suresh C. Ameta. "Photocatalytic degradation of fast green using nanosized CeCrO 3." *Macedonian Journal of Chemistry and Chemical Engineering* 29, no. 2 (2010): 195-202.

17) Bhati, Indu, Pinki B. Punjabi, and Suresh C. Ameta. "Photocatalytic degradation of fast green using nanosized CeCrO 3." *Macedonian Journal of Chemistry and Chemical Engineering* 29, no. 2 (2010): 195-202.
18) Sarkar, Shrabana, Nidia Torres Ponce, Aparna Banerjee, Rajib Bandopadhyay, Saravanan Rajendran, and Eric Lichtfouse. "Green polymeric nanomaterials for the photocatalytic degradation of dyes: a review." *Environmental Chemistry Letters* (2020): 1-12.
19) Kumar, P. Vijaya, A. Jafar Ahamed, and M. Karthikeyan. "Synthesis and characterization of NiO nanoparticles by chemical as well as green routes and their comparisons with respect to cytotoxic effect and toxicity studies in microbial and MCF-7 cancer cell models." *SN Applied Sciences* 1, no. 9 (2019): 1-15.
20) Vladár, András E., and Vasile-Dan Hodoroaba. "Characterization of nanoparticles by scanning electron microscopy." In *Characterization of Nanoparticles*, pp. 7-27. Elsevier, 2020.
21) Hodoroaba, Vasile-Dan, Steffi Rades, T. Salge, Johannes Mielke, Erik Ortel, and R. Schmidt. "Characterisation of nanoparticles by means of high-resolution SEM/EDS in transmission mode." In *IOP Conference Series: Materials Science and Engineering*, vol. 109, no. 1, p. 012006. IOP Publishing, 2016.
22) Baraton, Marie-Isabelle, and Lhadi Merhari. "Dual contribution of FTIR spectroscopy to nanoparticles characterization: surface chemistry and electrical properties." In *Nanomaterials Synthesis, Interfacing, and Integrating in Devices, Circuits, and Systems II*, vol. 6768, p. 676806. International Society for Optics and Photonics, 2007.
23) Preetha Devaraj, Prachi Kumari, Chirom Aarti,and Arun Renganathan, Synthesis and Characterization of Silver Nanoparticles Using Cannonball Leaves and Their Cytotoxic Activity against MCF-7 Cell Line; Journal of nanotechnology,2013
24) Qiao, Hongxia, Zhiqiang Wei, Hua Yang, Lin Zhu, and Xiaoyan Yan. "Preparation and characterization of NiO nanoparticles by anodic arc plasma method." *Journal of Nanomaterials* 2009 (2009).
25) Vladár, András E., and Vasile-Dan Hodoroaba. "Characterization of nanoparticles by scanning electron microscopy." In *Characterization of Nanoparticles*, pp. 7-27. Elsevier, 2020.
26) Halder, Mita, Md Mominul Islam, Pritam Singh, Anupam Singha Roy, Sk Manirul Islam, and Kamalika Sen. "Sustainable Generation of Ni (OH) 2 Nanoparticles for the Green Synthesis of 5-Substituted 1H-Tetrazoles: A Competent Turn on Fluorescence Sensing of H2O2." *ACS omega* 3, no. 7 (2018): 8169-8180.
27) Hashem, Manal, Elias Saion, Naif Mohammed Al-Hada, Halimah Mohamed Kamari, Abdul H. Shaari, Zainal Abidin Talib, Suriati B. Paiman, and Mazliana A. Kamarudeen. "Fabrication and characterization of semiconductor nickel oxide (NiO) nanoparticles manufactured using a facile thermal treatment." *Results in physics* 6 (2016): 1024-1030.
28) Heera, P., and S. Shanmugam. "Nanoparticle characterization and application: an overview." *Int. J. Curr. Microbiol. App. Sci* 4, no. 8 (2015): 379-386.
29) Srihasam, Saiganesh, Krishnan Thyagarajan, Mallikarjuna Korivi, Veeranjaneya Reddy Lebaka, and Siva Pratap Reddy Mallem. "Phytogenic generation of NiO nanoparticles using Stevia leaf extract and evaluation of their in-vitro antioxidant and antimicrobial properties." *Biomolecules* 10, no. 1 (2020): 89.
30) Yang, Chun-Chen. "Synthesis and characterization of active materials of Ni (OH) 2 powders." *International Journal of Hydrogen Energy* 27, no. 10 (2002): 1071-1081.
31) Kovalenko, Vadym, and Valerii Kotok. "The popcorn effect": obtaining of the highly active ultrafine nickel hydroxide by microwave treatment of wet precipitate." (2018): 12-20.
32) Sun S, Zhang Y-Chao, Shen G, Wang Y, Liu X, Duan Z, Pan L, Zhang X, Zou J-Jun, Photoinduced Composite of Pt decorated Ni(OH)2 as Strongly Synergetic Cocatalyst to Boost H2O Activation for Photocatalytic Overall Water Splitting, Applied Catalysis B: Environmental 243 (2019) 253-261.
33) Kumar DR, Ranjith KS, Nivedita LR, Asokan K, Rajendra Kumar RT Swift heavy ion induced effects on structural, optical and photo-catalytic properties of Ag irradiated vertically aligned ZnO nanorod arrays. Nucl Instruments Methods Phys Res Sect B Beam Interact with Mater Atoms 450 (2019) 95–99.